NANO LETTERS

Letter

pubs.acs.org/NanoLett

Internal Electron Tunneling Enabled Ultrasensitive Position/Force Peapod Sensors

Xinyong Tao,[†,∥] Zheng Fan,[‡] Bradley J. Nelson,[§] Gautham Dharuman,[‡] Wenkui Zhang,[∥] Lixin Dong,*[,‡] and Xiaodong Li*[,†,#]

[†]Department of Mechanical Engineering, University of South Carolina, 300 Main Street, Columbia, South Carolina 29208, United States

[‡]Department of Electrical and Computer Engineering, Michigan State University, East Lansing, Michigan 48824-1226, United States

[§]Institute of Robotics and Intelligent Systems, ETH Zurich, CH-8092 Zurich, Switzerland

[∥]College of Materials Science and Engineering, Zhejiang University of Technology, Hangzhou 310014, China

[#]Department of Mechanical and Aerospace Engineering, University of Virginia, Charlottesville, Virginia 22904-4746, United States

Supporting Information

ABSTRACT: The electron quantum tunneling effect guarantees the ultrahigh spatial resolution of the scanning tunneling microscope (STM), but there have been no other significant applications of this effect after the invention of STM. Here we report the implementation of electron-tunneling-based high sensitivity transducers using a peapod B_4C nanowire, where discrete Ni_6Si_2B nanorods are embedded in the nanowire in a peapod form. The deformation of the nanowire provides a higher order scaling effect between conductivity and deformation strain, thus allowing the potentials of position and force sensing at the picoscale.

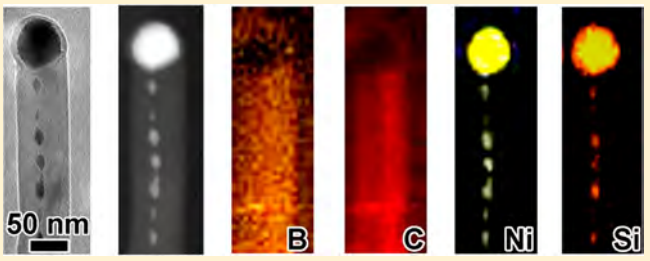

KEYWORDS: *Nanowire, boron carbide, internal tunneling, nanoelectromechanical system, peapod structure*

It has been 29 years since Gerd Binnig and Heinrich Rohrer won the Nobel Prize in Physics for inventing the scanning tunneling microscope (STM) with incompatible spatial resolution,[1] but there have been no significant innovations on this technology in recent years: a high resolution is still based on an ultrahigh vacuum environment, alignment is still necessary, and the vertical scanning range is limited to several nanometers. Is it possible to further improve upon this technology on these aspects? Can we realize the tunneling effect inside individual nanowires to invent a nanowire tunneling picoscope regardless of the conductivity of the sample, the vacuum environment, and the alignment? In addition, sub-nanometer to picometer position sensing has been an essential base for transducers such as piconewton force sensors, attogram mass flow sensors, and single molecule detectors.[2] However, it is a grand challenge to implant the same principle of the STM into high resolution transducers. An early attempt can be traced back to the first prototype of atomic force microscopes (AFMs); an STM had been used as the deflection detector, but it was soon replaced with the routinely used laser-lever system due to its large measurement range and readiness for fabrication and alignment.

Nowadays, nanomaterials are enabling the development of highly sensitive, low power, ultrafast electromechanical transducers.[2−30] A variety of nanoelectromechanical systems (NEMS) are being actively explored for high performance transducers capable of sensing ultrasmall forces,[6−13,28−31] masses,[2,14,15] or displacements.[6,16−20] Intriguing electromechanical properties have been observed in carbon nanotubes (CNTs),[2,8,9,15,20,21,24,31] Si nanowires,[10,17,22,23] and ZnO nanowires.[11,32,33] Commonly, the transducers utilize the piezoresistive or piezoelectric properties of these nanomaterials, that is, under a small strain, the conductance of the material changes with strain following a linear or quasi-linear relationship.[11,17,19,22,23] However, very little emphasis has been laid on the application of tunneling effect of sensing in the nanoscale.

In this work, we investigated the integration of alignment-free gaps into the nanowire, which were utilized as internal electron tunneling-based high sensitivity transducers (Figure 1a). The schematic of the proposed tunneling transducer has two aspects intrinsically different from that in conventional nanosystems: the sub-nanostructures rather than the overall nanostructures are to serve as functional elements and accordingly the coupling between them transforms from an external behavior into an internal one. Based on internal electron tunneling, a nanowire tunneling picoscope can be designed for sensing pico- to nanometer position or displace-

Received: June 15, 2015
Revised: September 13, 2015
Published: October 12, 2015

DOI: 10.1021/acs.nanolett.5b02362
Nano Lett. 2015, 15, 7281−7287

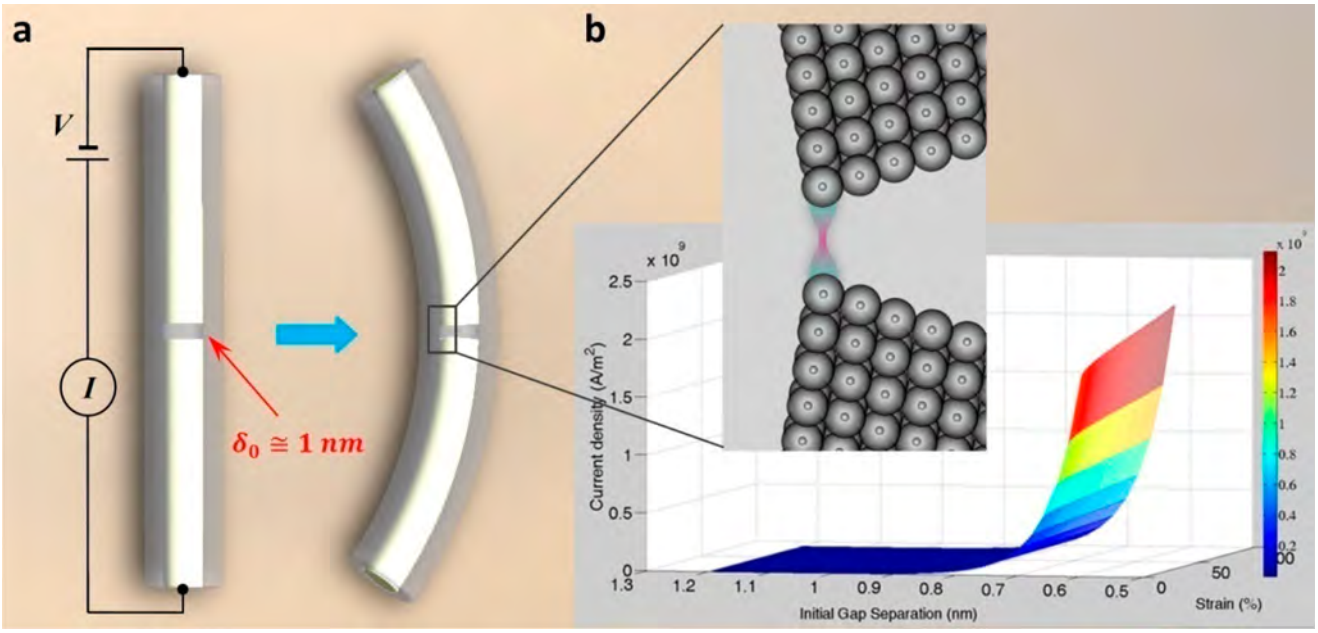

Figure 1. Model of the internal electron tunneling enabled transducer. (a) The schematic of the proposed tunneling-based force/displacement transducer. (b) The simulation of the tunneling performance on the proposed transducer with the dynamics of initial gap separations (δ_0) and external strains.

ment and piconewton forces. Among the nanowire-based displacement and force sensors, the ZnO nanowire-based nanopiezotronic devices have the advantage of fast response,[34,35] but this technique shows linear current response to the external displacement or force change. Here, due to the exponential change of the tunneling current according to the dynamics of inter-nanorod separation (Figure 1b), a much higher sensitivity than that by nanopiezotronic effect could be realized. Other stimuli such as heat and molecule induced stress can change the inter-nanorod separation; therefore highly sensitive temperature and molecular sensors can be designed with the same mechanism. Next, we will first introduce the simulation of the proposed tunneling transducer and then address the implementation of it.

We established a model of the buckling-induced tunneling effect in an individual gap-embedded nanowire (Figure S1) to quantitatively depict the mechanism of the proposed tunneling transducer. The proposed schematic simplifies the deformation of the nanowire as the buckling of a hinged−hinged attached beam.[36] The distance between two neighboring nanorods will decrease according to the buckling of the nanowire as well as its compression (Figure S1a). Here the reaction area was assumed to be the cross-sectional area of the metal atom (Figure 1b, inset). The translocation of electrons through the sub-nanometer separation triggers tunneling current, which varies exponentially with the change in distance. The buckling−tunneling model correlates well the tunneling current with the buckling-induced inter-nanorod separation change. Here we apply the tunneling metal−insulator−metal (MIM) model to the proposed nanowire system. The approximate expression of the tunneling current density is given by[37]

$$J = \frac{e}{2\pi\hbar\delta^2}[\bar{\Phi}_B\, e^{-(\sqrt{8m}/\hbar)\delta\sqrt{\bar{\Phi}_B}} - (\bar{\Phi}_B + eV)\, e^{-(\sqrt{8m}/\hbar)\delta\sqrt{\bar{\Phi}_B+eV}}] \quad (1)$$

where m is the mass of the electron, $\hbar$ is the Plank constant, $\bar{\Phi}_B$ is the average barrier height between the two electrodes, V is the voltage applied between the two electrodes, and δ is the inter-nanorod separation induced by the buckling strain, ε, which can be expressed as

$$\delta = \frac{lF(\Phi, p)}{K(p)}(1 - \varepsilon) - 2dp\,\mathrm{sn}\left[K(p)\left(\frac{x_0}{l}\right)\right]\sqrt{1 - p^2\,\mathrm{sn}^2\left[K(p)\left(\frac{x_0}{l}\right)\right]} \quad (2)$$

where l is the length of the nanowire, $F(\Phi, p)$ is the incomplete elliptic integral of the first kind, here $\Phi = \sin^{-1}(\sin(\theta/2)/p)$ and $p = \sin(\alpha/2)$, $K(p)$ symbolizes the variation of the terminal angle α, x_0 is half the length of the initial inter-nanorod separation, $\mathrm{sn}[u]$ is the Jacobi elliptic function, and $u = K(p)(x_0/l)$.

The tunneling simulations of the nanowire at different geometrical/physicochemical parameters were carried out. The simulations demonstrate that four parameters, external and inner wire diameter, initial gap separation, nanowire length, and the material work function will largely influence the tunneling performance of the proposed nanostructure (Figures S2−S5), which provides instructions for the implementation of the proposed tunneling transducer. Based on the simulations, the comparatively larger nanorod diameters, the smaller initial gap separation, comparatively shorter nanowire length, and higher conductivity of the nanorod will provide better tunneling performances.

To implement the proposed tunneling transducer, we synthesized a new type of B_4C peapod nanowire with alignment-free internal electron tunneling gaps. B_4C is an important ceramic material widely used in tank armors, aircraft armors, bulletproof vests, and numerous other industrial applications.[38] One-dimensional boron carbide nanostructures have attracted significant attention due to their exceptional

DOI: 10.1021/acs.nanolett.5b02362
Nano Lett. 2015, 15, 7281−7287

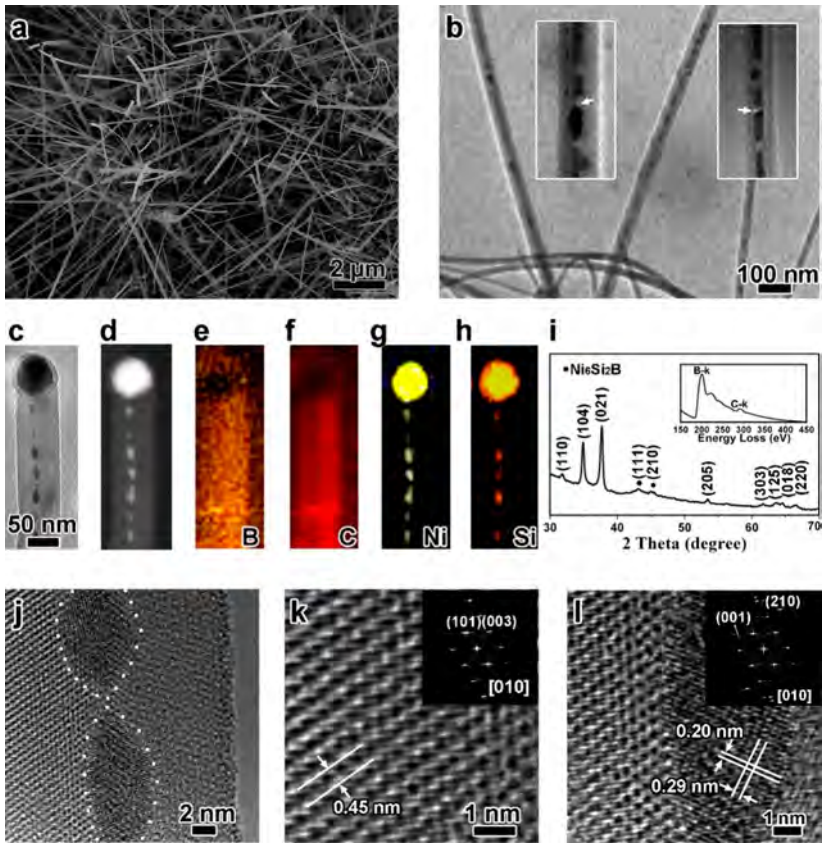

Figure 2. Microstructure and composition of the B_4C peapod nanostructures. (a) SEM image of the as-synthesized sample. (b) TEM image of the nanowires. Discrete nanorods with the unique cavity structures can be seen in the nanowire, as shown in the close-up view in the inset. (c) TEM image of a single nanowire with a catalyst particle on the tip. (d) The corresponding scanning transmission electron microscope (STEM) image of panel c. (e–h) Respective element distribution maps of B, C, Ni, and Si. (i) XRD pattern of the B_4C peapod nanostructures. The inset is a representative EELS spectrum taken from the nanostructure. (j) A representative HRTEM image of the B_4C peapod nanostructure. (k) The close-up view and the corresponding FFT pattern (the inset) of panel j. The electron beam irradiation direction is along [010] of B_4C. (l) The close-up view and the corresponding FFT pattern (the inset) of panel j, showing that the embedded nanorods are Ni_6Si_2B.

physical properties.[39,40] We found that such peapod B_4C nanostructures have similar schematics to the proposed transducer and exhibit a unique tunneling behavior upon bending or buckling deformation.

A representative scanning electron microscopy (SEM) image of the as-synthesized product (Figure 2a) indicates an abundance of straight nanowires. Different from the normal boron carbide nanowires,[39−43] there are discrete nanorods embedded in the individual nanowire (Figure 2b). Similar hybrid peapod structures have also been observed in the nanowires of Au-in-Ga_2O_3,[44] fullerenes-in-CNTs,[45] and Au-in-SiO_2.[46] As indicated by the arrows in the inset of Figure 2b, the transmission electron microscopy (TEM) image reveals that there are cavity structures between two adjacent nanorods. The nanowire terminates at the catalyst particle (Figure 2c,d) containing Ni (Figure 2g) and Si (Figure 2h). Respective element distribution maps (Figure 2e–h) reveal that B and C are rich in the stem of nanowire and the embedded nanorods have similar components to the catalyst particle. X-ray diffraction (XRD) spectrometry confirms that rhombohedral B_4C (JCPDF No. 35-0798) is the dominant phase (Figure 2i). The peaks at 43.1° and 45.3° can be indexed as (111) and (210) of nickel silicon boride Ni_6Si_2B (JCPDF No. 65-1991) with a hexagonal structure of Fe_2P-type (space group $P\bar{6}2m$, No. 189), which is an electrically conductive ternary compound.[47] The elemental mapping and XRD results jointly suggest that both the catalyst particles and the embedded nanorods are conductive Ni_6Si_2B phase. Two distinct absorption features at 188 and 284 eV in the electron energy loss spectrum (EELS) (see the inset in Figure 2i) correspond to the known B k- and C k-edges, respectively, indicating that the nanowire stem is B_4C. The high resolution TEM (HRTEM) images (Figure 2j–l) and the corresponding fast Fourier transform (FFT) diffraction pattern (insets in Figure 2k) jointly reveal that the B_4C nanowire stem is single crystalline. Figure 2l shows the close-up view and the corresponding FFT pattern (the inset) of the lower part of Figure 2j, validating that the embedded nanorods are Ni_6Si_2B. Since the Ni–Si–B system has a eutectic point lower than 1000 °C,[48] the Ni_6Si_2B nanorods must be in a molten or quasi-liquid state during the growth of the B_4C nanowire at 1160 °C. Moreover, B_4C has a low coefficient of thermal expansion ($(4-8) \times 10^{-6}$ °C^{-1}) and a high melting point (2350 °C). Therefore, upon solidification, the embedded Ni_6Si_2B nanorods shrink more than the B_4C nanowires, forming the unique cavity structures (hollow spaces between the embedded nanorods), as observed with TEM (Figure 2b).

The elastic modulus of B_4C peapod nanostructures was measured by a three-point-bending test (Figure S6). The 17 bending tests on the same peapod nanowire for the elastic modulus indicated that the peapod nanowire showed a robustness of the deformation and the nanowire structure

DOI: 10.1021/acs.nanolett.5b02362
Nano Lett. 2015, 15, 7281−7287

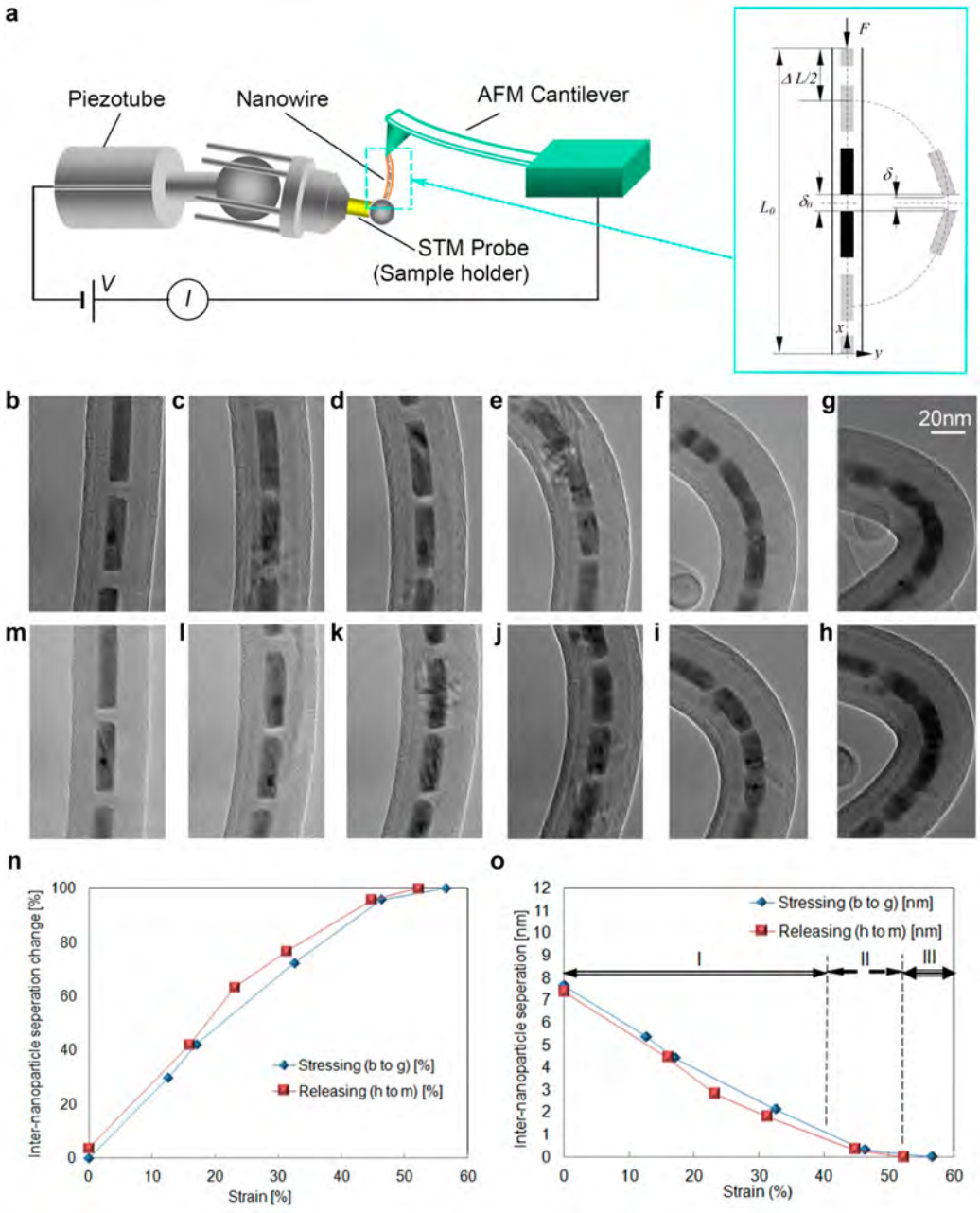

Figure 3. *In situ* buckling and electromechanical characterization of a B_4C peapod nanostructure inside a TEM. (a) Experimental setup. An STM built in a TEM holder serves as a nanomanipulator to manipulate the nanowire, and a conductive AFM cantilever was used to characterize the nanowires and measure the force applied on the nanowire. Inset, Schematic drawing of the nanowire before and after buckling. (b–m) The buckling process recorded by TEM images: stressing (b–g), releasing (h–m). (n) Relation between strain and the change of the inter-nanorod separation. (o) Relation between the strain and the inter-nanorod separation. Panels b–h share the same scale bar as shown in panel g.

was stabilized before and after the bending test, which provides the possibility of using the B_4C peapod nanowire as a reliable and robust nanowire transducer in the nanoscale.

To obtain detailed electromechanical properties, individual B_4C peapod nanostructures were buckled *in situ* for electromechanical characterization inside a TEM (Figure 3). A STM built in a TEM serves as a nanomanipulator (Figure 3a).[49−53] The details of the experiment setup of the STM unit are in Supporting Information. The representative buckling process was recorded with TEM images (Figure 3b–m), which include the bending process (Figure 3b–g) and the releasing one (Figure 3h–m). Surprisingly, the nanowire can be bent to a sharp angle (70°) with no apparent cracking or degradation for a strain up to 40.5%. It is well-known that bulk B_4C is brittle in nature, but at the nanometer-scale, B_4C peapod nanostructures appear ductile. Both the nanowires and the embedded nickel silicon boride nanorods were elastically deformed under multiple high-load bending steps without a brittle failure or obvious residual deformation (Figure 3b–m).

As the B_4C peapod nanostructure deforms, the separation between the encapsulated nanorods decreases. Based on the detailed geometry analysis of a peapod nanostructure as shown in the inset of Figure 3a, the chord length of the nanostructure becomes $L = L_0 - \Delta L$ when an external force F is applied. The strain ε is defined as a function of length change of ΔL over the original length L_0 under the approximation of homogeneous

DOI: 10.1021/acs.nanolett.5b02362
Nano Lett. 2015, 15, 7281−7287

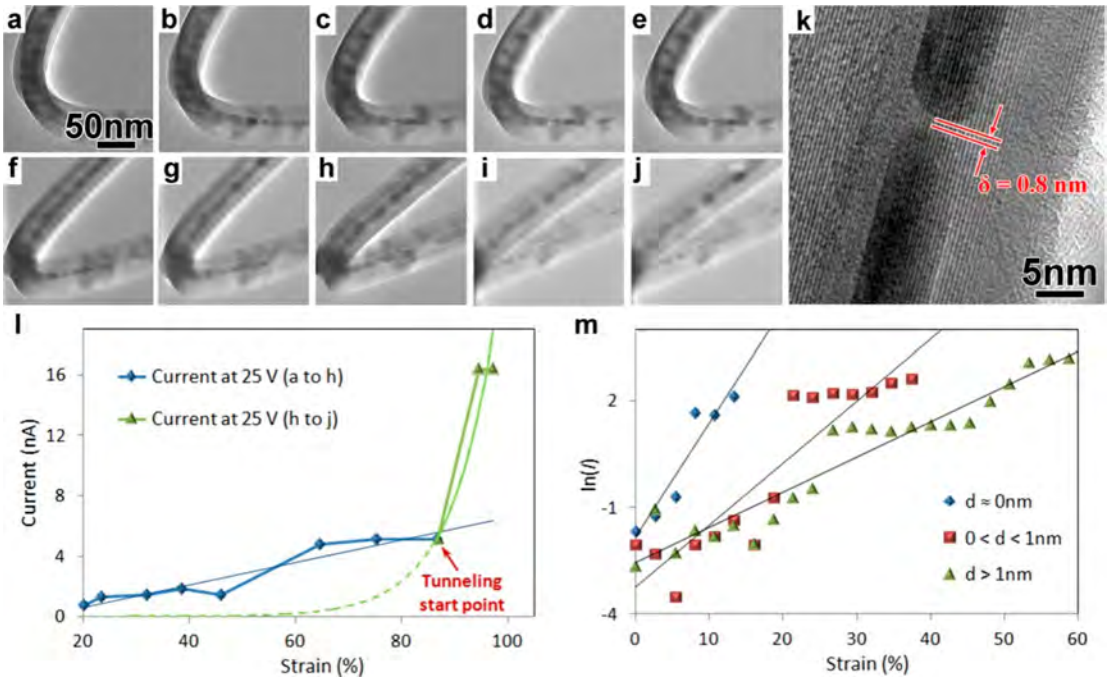

Figure 4. Force/displacement sensing with inter-nanorod tunneling effect in a B_4C peapod nanostructure. (a–j) The stressing process recorded with TEM images. (k) A HRTEM image shows that the inter-nanorod separation, δ, under the external stress can be smaller than 1 nm, which is appropriate for tunneling. (l) The relation between the current and the strain of the nanowire. The inter-nanorod current increases with the increase of external force at different rates under an external bias voltage of 25 V. At the low-stress stage, the current increases approximately linearly to the external force, and the strain-–urrent curve is fitted by $I = 0.0741\varepsilon - 0.8626$. However, starting from the point h on, the current jumps abruptly and increases with a quasi-exponential trend to the external force. This abrupt increase and the quasi-exponential trend strongly suggest that inter-nanorod tunneling occurred. In this case, the current–force curve in the high strain region (point h–j) fits well with an exponential curve: $I = 1 \times 10^{-4}\, e^{0.121\varepsilon}$. (m) Relations between the strain and the natural logarithm value of current in the B_4C nanostructures with different inter-nanorod gap distances. All curves fit with the linear trends (as $d \approx 0$ nm, $I = e^{0.3206\varepsilon - 1.8263}$, as $0 < d < 1$ nm, $I = e^{0.1748\varepsilon - 3.2491}$, and as $d > 1$ nm, $I = e^{0.0993\varepsilon - 2.555}$), thus showing the quasi-exponential relations.

strain, $\varepsilon = \Delta L/L_0$, and the inter-nanorod separation change is expressed as $s = (\delta_0 - \delta)/\delta_0$, where δ and δ_0 are the separation and its initial value, respectively. According to the *in situ* real-time images of the buckling process (Figure 3b–m), the strain vs inter-nanorod separation change can be depicted in Figure 3n. The relation between the strain and the inter-nanorod separation is depicted in Figure 3o. Three intervals "I", "II", and "III" are identified to represent the regimes in which the inter-nanorod separation is larger than approximately 1 nm, between 1 and 0 nm, and 0 nm, respectively.

On a practical level, the controlled inter-nanorod separation allows us to effectively couple the electrical property variation with external force/strain change. More importantly, this technique provides insights into the electronic transport properties of the peapod nanostructures and creates unprecedented opportunities for intersegment-based sensing. By adjusting the stress on the two ends of the nanowire, we can regulate the distance between the two neighboring nanorods in different regimes (regions I, II, and III). Then the nanowire will acquire different electronic structures, thus modulating its transport properties. The conductivity change of the nanowire was also recorded using a nanoampere meter during the buckling process.

The B_4C peapod nanostructure shows a piezoresistive transport characteristic (Figure S7a) as the inter-nanorod separation falls into region I (in Figure 3b,m, the average inter-nanorod gap is 7.7 nm). It is generally known that the band structure change contributes to the piezoresistive effect in common NEMS.[11,19,23,24] An important question arises: Does the piezoresistive effect also originate from the band structure change? To answer this question, comparative experiments were performed on individual B_4C nanowires without having embedded nickel silicon boride nanorods. The homogeneous B_4C nanowires exhibit higher resistance than the peapod nanostructures, and no piezoresistive effect was observed. It is well-known that nickel silicon boride is a good electrical conductor and B_4C has a relatively high resistance, indicating that the peapod B_4C nanostructure can function as a Coulomb blockade (CB)[54,55] chain. The B_4C thin walls, partnering together with the cavity between two adjacent conductive nanorods, act as tunneling junctions along the nanowire, forming a unique metal–insulator–metal (MIM) structure. Theoretical and experimental studies[1,37] on the electrical transport characteristics of nanojunction systems reveal that the tunneling effect exclusively depends on the inter-nanorod separation. Hence, the change in inter-nanorod separation can alter the tunneling transport configuration, which in turn affects the tunneling current. The piezoresistive effect dominates the tunneling effect in a junction with large separation, for instance, in region I, where the tunneling current remains low. The linear increase in current during buckling as a result of piezoresistive effect implies its potential for sensing position and strain change (Figure S7e).

As the bending strain increases, the inter-nanorod separation δ decreases down to a few angstroms (in region II) (Figure 4a–j). In this region, the inter-nanorod tunneling is accordingly enhanced and starts to dominate the conductivity until the strain forces the separated nanorods into region III. The

DOI: 10.1021/acs.nanolett.5b02362
Nano Lett. 2015, 15, 7281–7287

current density j_t changes exponentially with the inter-nanorod separation,[37] $j_t \sim e^{-\delta}$. If the initial separation δ_0 is in the sub-nanometer range, the tunneling can also occur at low strain (Figure 4k). Such an exponential increase can further amplify the strain-induced resistance change, providing an extremely high sensitivity to the position and force change. Here we demonstrate the transition from piezoresistive electron transport to tunneling electron transport due to the increased strain (Figure 4l). A linear current increase is illustrated at the low-stress stage under an external bias voltage of 25 V, and the current−strain (I−ε) curve was fitted by the equation $I = 0.0741\varepsilon - 0.8626$ (Figure 4l). Along with the increase in stress, the separation enters region II, the current jumps abruptly and increases with a quasi-exponential trend to the external force, and the conductivity is at least two orders of magnitude higher than that in the low-stress stage. This abrupt increase strongly implied the beginning of inter-nanorod tunneling (Figure 4h−j). The I−ε curve in the high strain region is fitted by an exponential curve: $I = 1 \times 10^{-4}\, e^{0.121\varepsilon}$ (Figure 4l). To further prove the reproducibility of the tunneling effect in peapod B_4C nanostructures, we have characterized the relations between the strain and current with different inter-nanorod gap distances (Figure 4m). All curves show the quasi-exponential trend under an external bias voltage of 25 V. Since each inter-nanorod gap could be regarded as an equivalent resistance along the nanowire, the peapod nanostructure is the series connection of such gaps. Therefore, the bias applied on the peapod nanowire for the tunneling (e.g., V) should be associated with the numbers of the gaps (e.g., n) embedded in the nanowire and the minimum bias for initiating the tunneling performance (e.g., V/n) in a single gap. Because there are about 10 gaps connected in series along the nanowire (Figure 4a), we reduced the bias voltage to 2.5 V for an individual gap to simulate the tunneling behavior. As shown in Figure S2, the maximum current density reaches 6×10^7 A/m^2 as the inner nanorod is about 20 nm. Then the tunneling peak current could be calculated as 18.9 nA. Moreover, the results achieved in the *in situ* experiment on the nanowire with similar structure schematic to the simulated model (Figure 4i) show that the peak tunneling current is about 16 nA, which is consistent with the model prediction and also indicates that the tunneling behavior that we observed in a nanowire is in strong agreement with the proposed mechanism, which further verifies the assumption regarding the tunneling reaction on the cross-section of a metal atom that we made in the previous paragraph.

The B_4C peapod nanostructures were enabled with the capability of simple, highly sensitive displacement, force, and strain sensing from the encapsulated tunneling gap. Furthermore, due to the series arrangement of the nanorods along the nanowire, the peapod nanowire is provided with a more robust and stable structure than the individual gap-embedded nanowire, which easily generates a kink other than buckling during the bending process. Therefore, the peapod nanowire is an ideal implementation of the proposed tunneling transducer model and shows the potential for sensing the force and displacement down to piconewton or picometer level. In addition, a variety of nanostructures, such as CNTs and graphene, can be tailored into segmented ones via shell/layer engineering, whereas the combinations of the materials of peas and pods are unlimited.

In summary, we have demonstrated a model of a tunneling transducer with internal electron tunneling enabled electromechanical coupling. A new type of B_4C nanowire with a unique peapod structure was developed for the implementation of the proposed tunneling transducer. The peapod B_4C nanowires exhibited elastically recoverable deformation after multiple high-strain bending cycles without an apparent brittle failure or obvious residual deformation. The long-term reliability and the effect of the possible inelastic deformation on the performance of the sensor will be studied further in our following work. From the measurements, we have also determined the Young's modulus of peapod B_4C nanostructures, which is an important parameter of these unique building blocks for practical applications. The tunneling effect from the neighboring nanorods in the peapod nanostructure enables the potential of simultaneous position and force sensing at the picometer and piconewton levels. These findings open a new ground for developing electron tunneling nano- or picoscopes, nano- or picosensors, and smart nanocomposites, opening up the possibility of discovering new phenomena in a wide range of fields, such as measuring the adhesion forces of cells on extracellular matrix substrates or shear forces in microfluidic applications.

■ ASSOCIATED CONTENT

Supporting Information

The Supporting Information is available free of charge on the ACS Publications website at DOI: 10.1021/acs.nanolett.5b02362.

Detailed description of the experimental procedures and calculations (PDF)

■ AUTHOR INFORMATION

Corresponding Authors

*E-mail: ldong@egr.msu.edu (L.D.).
*E-mail: xl3p@virginia.edu (X.L.).

Present Address

Z.F.: Department of Materials Science and Engineering and California NanoSystems Institute (CNSI), University of California, Los Angeles, CA 90095, USA.

Author Contributions

⊥X.T., Z.F., L.D. and X.L. contributed equally to this work. X.T., L.D. and X.L. conceived the idea. X.T. carried out the material synthesis and microstructure analysis. L.D. and Z.F. performed the *in situ* TEM electromechanical measurements. Z.F., G.D. and L.D. carried out the modeling. All the authors discussed the results and commented on the manuscript.

Notes

The authors declare no competing financial interest.

■ ACKNOWLEDGMENTS

The authors thank Douglas Blom and Soumitra Ghoshroy (the University of South Carolina EM Center) for TEM technical support. Financial support for this study was provided by the National Science Foundation (Grants IIS-1054585, CMMI-1129979, and CMMI-0968843), the ACS Petroleum Research Fund (Grant ACS PRF 40450-AC10), National Natural Science Foundation of China (Grants 51002138 and 51172205), New Century Excellent Talents in University (Grant NCET 111079), and the Natural Science Foundation of Zhejiang Province (Grant LR13E020002).

DOI: 10.1021/acs.nanolett.5b02362
Nano Lett. 2015, 15, 7281−7287

REFERENCES

(1) Binnig, G.; Rohrer, H.; Gerber, C.; Weibel, E. *Phys. Rev. Lett.* **1982**, *49*, 57−61.
(2) Jensen, K.; Kim, K.; Zettl, A. *Nat. Nanotechnol.* **2008**, *3*, 533−537.
(3) Cui, Y.; Wei, Q. Q.; Park, H. K.; Lieber, C. M. *Science* **2001**, *293*, 1289−1292.
(4) Kang, D.; Pikhitsa, P. V.; Choi, Y. W.; Lee, C.; Shin, S. S.; Piao, L. F.; Park, B.; Suh, K. Y.; Kim, T. I.; Choi, M. *Nature* **2014**, *516*, 222−226.
(5) Nguyen, T. D.; Mao, S.; Yeh, Y. W.; Purohit, P. K.; McAlpine, M. C. *Adv. Mater.* **2013**, *25*, 946−974.
(6) Reserbat-Plantey, A.; Marty, L.; Arcizet, O.; Bendiab, N.; Bouchiat, V. *Nat. Nanotechnol.* **2012**, *7*, 151−155.
(7) Pang, C.; Lee, G. Y.; Kim, T. I.; Kim, S. M.; Kim, H. N.; Ahn, S. H.; Suh, K. Y. *Nat. Mater.* **2012**, *11*, 795−801.
(8) Lima, M. D.; Li, N.; de Andrade, M. J.; Fang, S. L.; Oh, J.; Spinks, G. M.; Kozlov, M. E.; Haines, C. S.; Suh, D.; Foroughi, J.; Kim, S. J.; Chen, Y. S.; Ware, T.; Shin, M. K.; Machado, L. D.; Fonseca, A. F.; Madden, J. D. W.; Voit, W. E.; Galvao, D. S.; Baughman, R. H. *Science* **2012**, *338*, 928−932.
(9) Lipomi, D. J.; Vosgueritchian, M.; Tee, B. C. K.; Hellstrom, S. L.; Lee, J. A.; Fox, C. H.; Bao, Z. N. *Nat. Nanotechnol.* **2011**, *6*, 788−792.
(10) Takei, K.; Takahashi, T.; Ho, J. C.; Ko, H.; Gillies, A. G.; Leu, P. W.; Fearing, R. S.; Javey, A. *Nat. Mater.* **2010**, *9*, 821−826.
(11) Zhou, J.; Gu, Y. D.; Fei, P.; Mai, W. J.; Gao, Y. F.; Yang, R. S.; Bao, G.; Wang, Z. L. *Nano Lett.* **2008**, *8*, 3035−3040.
(12) Rugar, D.; Budakian, R.; Mamin, H. J.; Chui, B. W. *Nature* **2004**, *430*, 329−332.
(13) Zhou, Y. S.; Hinchet, R.; Yang, Y.; Ardila, G.; Songmuang, R.; Zhang, F.; Zhang, Y.; Han, W. H.; Pradel, K.; Montes, L.; Mouis, M.; Wang, Z. L. *Adv. Mater.* **2013**, *25*, 883−888.
(14) Fritz, J.; Baller, M. K.; Lang, H. P.; Rothuizen, H.; Vettiger, P.; Meyer, E.; Guntherodt, H. J.; Gerber, C.; Gimzewski, J. K. *Science* **2000**, *288*, 316−318.
(15) Chaste, J.; Eichler, A.; Moser, J.; Ceballos, G.; Rurali, R.; Bachtold, A. *Nat. Nanotechnol.* **2012**, *7*, 301−304.
(16) Doll, J. C.; Peng, A. W.; Ricci, A. J.; Pruitt, B. L. *Nano Lett.* **2012**, *12*, 6107−6111.
(17) He, R. R.; Feng, X. L.; Roukes, M. L.; Yang, P. D. *Nano Lett.* **2008**, *8*, 1756−1761.
(18) LaHaye, M. D.; Buu, O.; Camarota, B.; Schwab, K. C. *Science* **2004**, *304*, 74−77.
(19) Stampfer, C.; Jungen, A.; Linderman, R.; Obergfell, D.; Roth, S.; Hierold, C. *Nano Lett.* **2006**, *6*, 1449−1453.
(20) Yamada, T.; Hayamizu, Y.; Yamamoto, Y.; Yomogida, Y.; Izadi-Najafabadi, A.; Futaba, D. N.; Hata, K. *Nat. Nanotechnol.* **2011**, *6*, 296−301.
(21) Tombler, T. W.; Zhou, C. W.; Alexseyev, L.; Kong, J.; Dai, H. J.; Liu, L.; Jayanthi, C. S.; Tang, M. J.; Wu, S. Y. *Nature* **2000**, *405*, 769−772.
(22) Neuzil, P.; Wong, C. C.; Reboud, J. *Nano Lett.* **2010**, *10*, 1248−1252.
(23) He, R. R.; Yang, P. D. *Nat. Nanotechnol.* **2006**, *1*, 42−46.
(24) Hall, A. R.; Falvo, M. R.; Superfine, R.; Washburn, S. *Nat. Nanotechnol.* **2007**, *2*, 413−416.
(25) Feng, X. L.; White, C. J.; Hajimiri, A.; Roukes, M. L. *Nat. Nanotechnol.* **2008**, *3*, 342−346.
(26) Lee, J. O.; Song, Y. H.; Kim, M. W.; Kang, M. H.; Oh, J. S.; Yang, H. H.; Yoon, J. B. *Nat. Nanotechnol.* **2013**, *8*, 36−40.
(27) Dagdeviren, C.; Su, Y. W.; Joe, P.; Yona, R.; Liu, Y. H.; Kim, Y. S.; Huang, Y. A.; Damadoran, A. R.; Xia, J.; Martin, L. W.; Huang, Y. G.; Rogers, J. A. *Nat. Commun.* **2014**, *5*, 4496.
(28) Ndieyira, J. W.; Kappeler, N.; Logan, S.; Cooper, M. A.; Abell, C.; McKendry, R. A.; Aeppli, G. *Nat. Nanotechnol.* **2014**, *9*, 225−232.
(29) Gong, S.; Schwalb, W.; Wang, Y. W.; Chen, Y.; Tang, Y.; Si, J.; Shirinzadeh, B.; Cheng, W. L. *Nat. Commun.* **2014**, *5*, 3132.
(30) Pan, L. J.; Chortos, A.; Yu, G. H.; Wang, Y. Q.; Isaacson, S.; Allen, R.; Shi, Y.; Dauskardt, R.; Bao, Z. N. *Nat. Commun.* **2014**, *5*, 3002.
(31) Yeom, C.; Chen, K.; Kiriya, D.; Yu, Z. B.; Cho, G.; Javey, A. *Adv. Mater.* **2015**, *27*, 1561−1566.
(32) Qin, Y.; Wang, X. D.; Wang, Z. L. *Nature* **2008**, *451*, 809−U5.
(33) Wang, Z. L. *Adv. Mater.* **2012**, *24*, 4632−4646.
(34) Hughes, W. L.; Wang, Z. L. *Appl. Phys. Lett.* **2003**, *82*, 2886−2888.
(35) Wang, Z. L. *Mater. Sci. Eng., R* **2009**, *64*, 33−71.
(36) Timoshenko, S. P.; Gere, J. M. *Theory of Elastic Stability*, 2nd ed.; McGraw-Hill: New York, 1961.
(37) Simmons, J. G. *J. Appl. Phys.* **1963**, *34*, 1793−1803.
(38) Chen, M. W.; McCauley, J. W.; Hemker, K. J. *Science* **2003**, *299*, 1563−1566.
(39) Tao, X. Y.; Li, Y. P.; Du, J.; Xia, Y.; Yang, Y. C.; Huang, H.; Gan, Y. P.; Zhang, W. K.; Li, X. D. *J. Mater. Chem.* **2011**, *21*, 9095−9102.
(40) Tao, X. Y.; Dong, L. X.; Wang, X. N.; Zhang, W. K.; Nelson, B. J.; Li, X. D. *Adv. Mater.* **2010**, *22*, 2055−2059.
(41) Welna, D. T.; Bender, J. D.; Wei, X. L.; Sneddon, L. G.; Allcock, H. R. *Adv. Mater.* **2005**, *17*, 859−862.
(42) Ma, R.; Bando, Y. *Chem. Mater.* **2002**, *14*, 4403−4407.
(43) Dai, H. J.; Wong, E. W.; Lu, Y. Z.; Fan, S. S.; Lieber, C. M. *Nature* **1995**, *375*, 769−772.
(44) Chen, P. H.; Hsieh, C. H.; Chen, S. Y.; Wu, C. H.; Wu, Y. J.; Chou, L. J.; Chen, L. J. *Nano Lett.* **2010**, *10*, 3267−3271.
(45) Utko, P.; Ferone, R.; Krive, I. V.; Shekhter, R. I.; Jonson, M.; Monthioux, M.; Noe, L.; Nygard, J. *Nat. Commun.* **2010**, *1*, 37.
(46) Hu, M. S.; Chen, H. L.; Shen, C. H.; Hong, L. S.; Huang, B. R.; Chen, K. H.; Chen, L. C. *Nat. Mater.* **2006**, *5*, 102−106.
(47) Colinet, C.; Tedenac, J. C. *Intermetallics* **2012**, *24*, 73−78.
(48) Tokunaga, T.; Nishio, K.; Hasebe, M. *J. Phase Equilib.* **2001**, *22*, 291−299.
(49) Dong, L. X.; Tao, X. Y.; Zhang, L.; Zhang, X. B.; Nelson, B. J. *Nano Lett.* **2007**, *7*, 58−63.
(50) Fan, Z.; Tao, X.; Fan, X.; Zhang, X.; Dong, L. *Carbon* **2015**, *86*, 280−287.
(51) Fan, Z.; Tao, X. Y.; Cui, X. D.; Fan, X. D.; Zhang, X. B.; Dong, L. X. *Nanoscale* **2012**, *4*, 5673−5679.
(52) Fan, Z.; Tao, X.; Fan, X.; Li, X.; Dong, L. *Robotics, IEEE Transactions on* **2015**, *31*, 12−18.
(53) Fan, Z.; Fan, X.; Li, A.; Dong, L. *Nanoscale* **2013**, *5*, 12310−12315.
(54) Park, J.; Pasupathy, A. N.; Goldsmith, J. I.; Chang, C.; Yaish, Y.; Petta, J. R.; Rinkoski, M.; Sethna, J. P.; Abruna, H. D.; McEuen, P. L.; Ralph, D. C. *Nature* **2002**, *417*, 722−725.
(55) Livermore, C.; Crouch, C. H.; Westervelt, R. M.; Campman, K. L.; Gossard, A. C. *Science* **1996**, *274*, 1332−1335.

DOI: 10.1021/acs.nanolett.5b02362
Nano Lett. 2015, 15, 7281−7287